Nanoscale Advances

ROYAL SOCIETY OF CHEMISTRY

REVIEW

View Article Online
View Journal | View Issue

Cite this: *Nanoscale Adv.*, 2025, **7**, 4535

A review of interface optimization strategies for solid electrolytes and anode materials

Dandan Wang,[ab] Xinyang Wu,[ab] Yongpeng Ren,[*abc] Yaru Li,[*ab] Xiaolin Xie,[c] Xiqiang Ma,[c] Ihar Razanau,[d] Xuemin Chen,[ab] Junhao Lu[ab] and Kunming Pan[abc]

With the increasing demand for high-performance power batteries in electric vehicles, low-altitude economy, military applications, and other fields, existing liquid electrolyte-based battery technologies are gradually becoming incapable of meeting the energy density and safety requirements. New battery systems based on solid electrolytes are the main candidate materials for future power batteries owing to their high safety and energy density. Thus far, researchers have conducted extensive studies on the ionic/electronic transfer mechanisms of solid electrolytes and electrode materials, as well as the cooperative effects and interface issues between them. Although much progress has been made, the practical application of solid-state batteries is still severely limited by the high interface impedance between the solid electrolyte and the anode. This impedance stems from incompatible physical and chemical properties and dynamic interface evolution. This paper focuses on the latest progress in the interface engineering strategies of solid electrolytes and anodes and systematically analyzes the cooperative coupling effect between charge transfer dynamics and mechanical stability at the interface. This review provides insights into the future research in this field, aiming to offer a new perspective to enhance our understanding of solid-state lithium batteries, thereby facilitating their more optimal design and promoting their practical applications.

Received 28th March 2025
Accepted 7th May 2025

DOI: 10.1039/d5na00286a

rsc.li/nanoscale-advances

1. Introduction

Driven by the rapid development of new energy vehicles, the installation of power batteries in China has shown a continuous upward trend. However, the explosive growth in sales of new energy vehicles has highlighted energy density and safety issues in traditional high-performance lithium batteries. Flammable organic liquid electrolytes (LEs) can easily heat up, decompose, and swell under abnormal conditions such as overcharging and short circuits, leading to thermal runaway. Additionally, liquid lithium-ion batteries are limited by their system, with a maximum energy density of only 300 Wh kg^{-1}, which struggles to meet the increasing performance demands of power batteries.[1–4] To simplify battery design while pursuing more efficient and safer batteries, solid-state batteries came into being.

Solid-state electrolytes (SSEs) are the core component of solid-state batteries, replacing flammable traditional organic LEs. SSEs possess mechanical strength that effectively mitigates the safety risks associated with lithium dendrites, fundamentally reducing the risk of battery fires and explosions. Most SSEs maintain good ion transport capabilities in both low- and high-temperature environments, ensuring stable operation of solid-state batteries across a wide temperature range, which further enhances battery cycle stability.[4,5] Additionally, SSEs are compatible with more reactive anode materials, such as lithium, and have a lighter weight, which can further enhance battery energy density. Although LEs exhibit good interfacial wettability and low interfacial impedance, the solid–solid interface between SSEs and electrodes suffers from high interfacial impedance, which significantly hinders Li^+ transport across the interface.[6] Therefore, the electrolyte–electrode interface issue is a critical challenge that urgently needs to be addressed in the field of solid-state batteries. In contrast to the cathode interface, the electrolyte–anode interface faces a range of challenges, including the formation of lithium dendrites, substantial volume changes, and various side reactions. These factors lead to unstable interface structures and limited ion transport, posing a greater challenge to optimizing solid-state battery performance, especially in high energy density anode material systems.[7,8]

Although lithium metal and silicon based anode materials are considered ideal anode materials for solid-state batteries due to their high specific capacity and low reduction potential, their inherent properties exacerbate the instability of the electrolyte–anode interface. For example, the high theoretical capacity of lithium metal anodes leads to continuous

[a]*School of Materials Science and Engineering, Henan University of Science and Technology, Luoyang 471000, China*
[b]*Henan Key Laboratory of High-temperature Structural and Functional Materials, Henan University of Science and Technology, Luoyang 471003, China*
[c]*Longmen Laboratory, Luoyang 471000, China*
[d]*Laboratory of Physical-Chemical Technologies, Scientific-Practical Materials Research Centre of National Academy of Sciences of Belarus, Minsk 220072, Belarus*

dissolution and deposition of active lithium, while the significant volume expansion of silicon anodes during lithiation leads to a vicious cycle of mechanical stress accumulation and interfacial chemical instability. Problems such as side reactions at the solid-state electrolyte–anode interface, instability of the anode solid electrolyte interphase (SEI) layer, and restricted ion transport at the interface severely impact the electrochemical performance and safety of solid-state batteries.[9–11] Therefore, it is very important to study and solve the problem of the electrolyte–anode interface for the construction of a high-performance solid-state battery system. In response to this, this paper offers a comprehensive review of the research progress on the solid-state electrolyte–anode interface in lithium batteries. It systematically examines the challenges and underlying mechanisms encountered by solid-state electrolytes, anode materials, and their interfaces. The goal is to elucidate design strategies and methods for optimizing electrolytes, anodes, and interfaces for next-generation high-performance solid-state batteries, ultimately facilitating their large-scale deployment.

2. Solid-state electrolytes (SSEs)

SSEs have the advantages of low volatility, high temperature resistance, corrosion resistance, chemical stability and excellent mechanical properties, and higher safety compared with LEs. They are also compatible with high-energy-density systems, with streamlined battery construction and enhanced energy density.[12–14] Currently, SSEs are primarily categorized into inorganic solid electrolytes (ISEs), solid polymer electrolytes (SPEs), and composite solid polymer electrolytes (CSPEs) (Fig. 1).[15]

2.1 Inorganic solid electrolytes (ISEs)

Inorganic solid electrolytes (ISEs) exhibit high ionic conductivity, thermal stability, Young's modulus, and safety. However, they face challenges such as the high interface impedance of the electrodes and the difficulty of handling thin ISE layers, which often require pressure to be applied during testing. Based on the choice of electrolyte materials, ISEs can be categorized into three types: oxides, sulfides, and halides.

2.1.1 Oxide-based solid-state electrolytes. An oxide-based solid electrolyte has excellent ionic conductivity and electrochemical stability, but it has rigidity and brittleness, poor contact with the electrode interface, and it is difficult to effectively alleviate the volume effect of the anode material during cycling.[17] In 2007, Murugan *et al.* synthesized LLZO ($Li_7La_3Zr_2O_{12}$) for the first time by the solid-state method, and its ion/electron conductivity at RT is 10^{-3} and 10^{-8} S cm^{-1}, respectively.[18] However, due to the existence of the Li^+ insulation layer composed of LiOH and Li_2CO_3, obvious polarization occurs in the process of lithium decolation, and lithium dendrites are produced. Kravchyk *et al.* improved interfacial contact by coating LLZO with metallic antimony (Sb), resulting in the formation of a Li–Sb alloy intermediate phase that reduced interfacial impedance to 4.1 Ω cm^{-2}.[19] The performance limitations of LLZO led to the development of tantalum-doped LLZTO ($Li_7La_3Zr_{2-x}Ta_xO_{12}$). Compared with LLZO, LLZTO has higher ionic conductivity, a wider electrochemical stability window and stronger chemical stability. Chen *et al.* developed a hybrid conductive layer composed of Li_3N and Li-in alloys, which has good stability of lithium metal and a high Li^+ diffusion coefficient, which can promote uniform lithium deposition, inhibit interface side reactions, and improve the stability of the LLZ/Li interface.[20]

In addition, strategies such as enhancing the flexibility of the electrolyte,[21] reducing the surface roughness,[22] and coating or modifying the electrolyte surface[23] can improve the interface contact with the anode and promote the application of oxide solid electrolytes in solid-state batteries. Future research will continue to address the core challenges of interface contact, using strategies such as element doping, grain boundary modification, and the construction of composite electrolytes to reduce interface impedance.

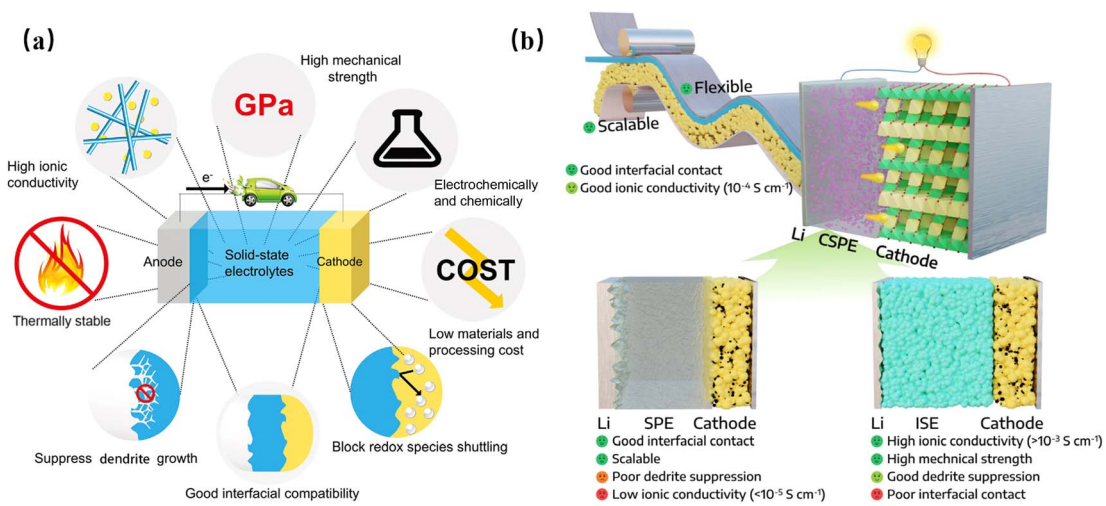

Fig. 1 (a) Characteristics of ideal solid-state electrolytes[16] and (b) classification.[15]

2.1.2 Sulfide-based solid-state electrolytes. Sulfide-based solid electrolytes exhibit excellent ionic conductivity and have significant advantages in superior machinability and flexibility compared with oxide-based solid electrolytes. Although they are regarded as core materials for next-generation batteries, interfacial side reactions remain a critical bottleneck hindering their practical application.[24–26] For example, when in contact with lithium metal, the sulfide electrolyte can be reduced to form a low ionic conductivity interface layer containing Li_2S and Li_3P, and is easily oxidized under high pressure, further degrading the interface. Lee *et al.* developed a silicon-based all-solid-state battery using a 3D nanorod silicon anode and $77.5Li_2S$-$22.5P_2S_5$ electrolyte, which effectively mitigated the volume expansion of the silicon anode during the cycle and maintained a high capacity retention rate after 20 cycles.[27] Focusing on the core issues of interface side reaction of the sulfide solid electrolyte, the practical application of sulfide solid batteries will be promoted from the aspects of sulfide and electrode modification, interface modeling and analysis, construction of composite electrolyte and composite electrode, cell design and so on (Fig. 2).

2.1.3 Halide-based solid-state electrolytes. Halide-based solid electrolytes are considered ideal candidates for solid-state electrolyte materials due to their exceptional ionic conductivity and broad electrochemical window, which render them suitable for a variety of electrode systems.[31] However, the high reduction potential and poor chemical stability seriously restrict its practical application in all-solid-state batteries. To address this interfacial stability challenge, Ji *et al.* used Li_6PS_5Cl as a protective layer to stabilize the interface between halide Li_3YCl_6 and lithium metal anode by generating an interface phase composed of Li_3P (10^{-4} S cm^{-1}) and insulated LiCl and Li_2S, thus effectively inhibiting the interface side reaction.[32] Although halogen-based solid electrolytes are being explored, oxide and sulfide materials currently dominate the field. Compared with oxides and sulfides, there is still a gap in the application potential of halides. Future advancements will further enhance the scalability of halide materials, including enhancing ionic conductivity, developing 2D/composite electrolyte films, and improving (electro)chemical stability.

2.2 Solid polymer electrolytes (SPEs)

SPEs primarily consist of polymer matrices (such as PEO) and lithium salts (like LiTFSI, LiDFOB, and $LiPF_6$). Flexible polymer chains have the advantages of good flexibility and adaptability. These polymer chains can adjust to various electrode interfaces through the movement and entanglement of molecular segments, ensuring a close fit to the electrode surface while maintaining efficient ionic transport pathways.[33,34]

2.2.1 PEO-based solid electrolytes. PEO (polyethylene oxide) is a polymer with flexible chain segments. Its molecular chain is connected by multiple ethylene oxide units and has a large number of strong polar ether-oxygen bonds, which can not only achieve close contact with the electrode surface, but also promote the uniform deposition of Li^+ during charge and

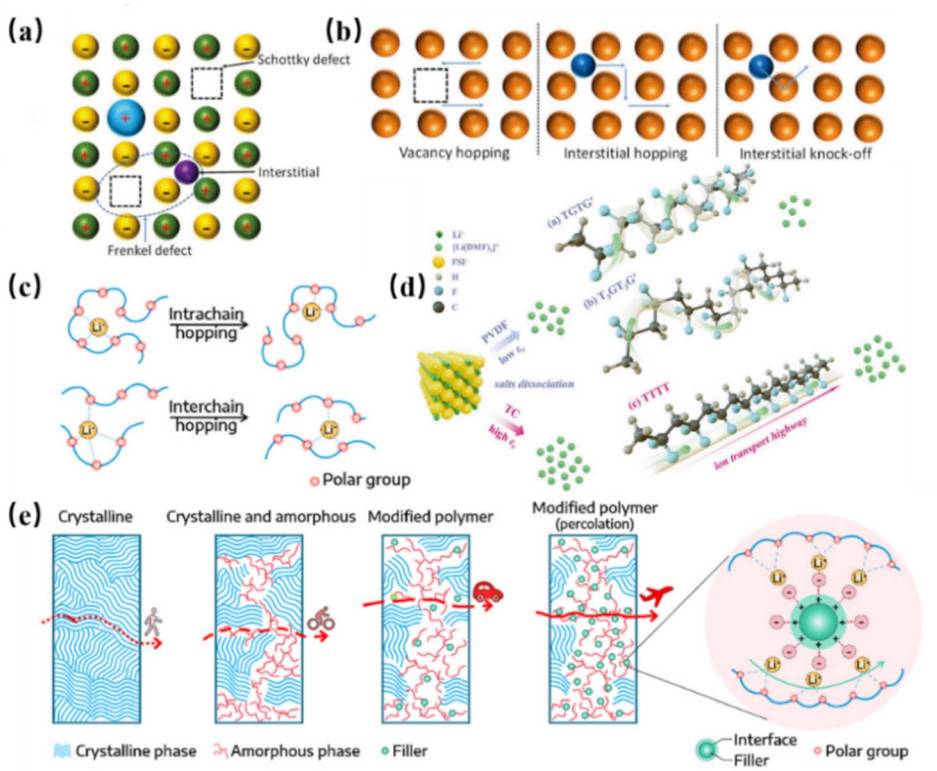

Fig. 2 (a) Typical defects[28] and (b) schematic of Li^+ transport in ISEs.[29] (c) Ion transport mechanism in SPEs.[15] (d) Schematic of lithium salt dissociation and ion transport facilitated by different permittivity and SPE conformation.[30] (e) Schematic of Li^+ diffusion in different SPEs.[15]

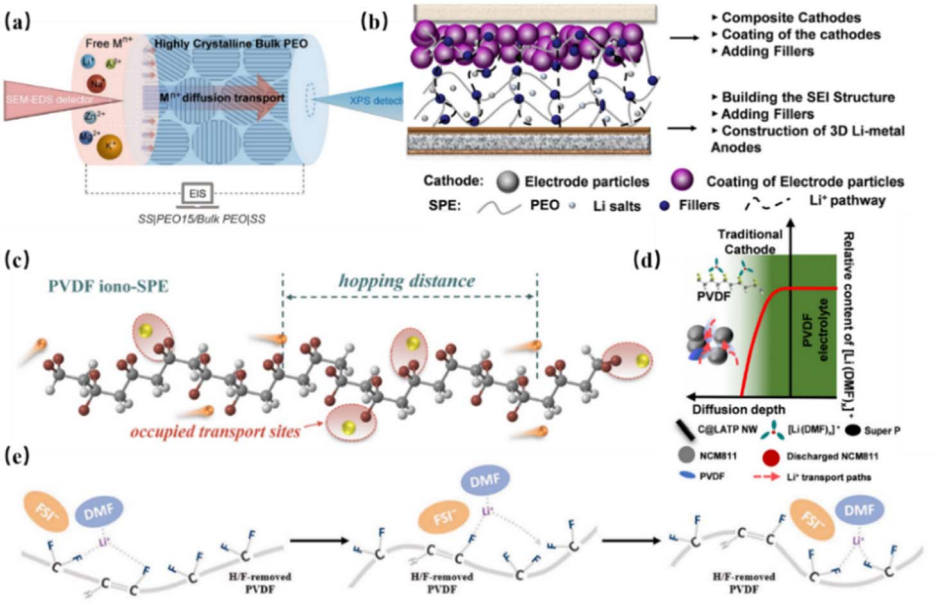

Fig. 3 (a) Schematic of ion diffusion in highly crystalline PEO.[36] (b) Schematic of the PEO-based electrolyte interface and performance enhancement.[43] (c) Schematic representation of Li^+ transport in the PVDF-based electrolyte.[44] (d) Diffusion of $[Li(DMF)_x]^+$ in P-NCM cathodes.[45] (e) Transport mechanism of $[Li(DMF)_x]^+$ in residual DMF solvent within the PVDF-based electrolyte.[41]

discharge.[35] However, the low ionic conductivity, narrow electrochemical window and insufficient thermal stability greatly limit its application. Li *et al.* discovered an adaptive ion diffusion phenomenon for Li^+, Na^+, K^+, and Mg^{2+} ions in highly crystalline PEO, proposing its use as an intermediate solid electrolyte layer. When matched with $LiFePO_4$, it has an 89% capacity retention rate after 2000 cycles at 1C.[36] Additionally, Wang *et al.* enhanced the interface compatibility by introducing electron-withdrawing Mg^{2+} and Al^{3+} into PEO, which weakened the strong reactivity of the EO groups with the $LiNi_{0.83}Co_{0.12}Mn_{0.05}O_2$ (Ni83) cathode at 4.8 V.[37] Yang *et al.* combined PBO nanofibers with PEO and LiTFSI to create rapid Li^+ conduction pathways, enhancing the ionic conductivity and mechanical strength of the electrolyte while effectively suppressing lithium dendrite growth.[35] In the future, it is still necessary to further improve the ionic conductivity and electrochemical stability of PEO-based solid electrolytes, continue studying the ion transport mechanism, and optimize the interaction with inorganic fillers to solve the interface problem with the anode, and realize its wide application in high energy density solid state batteries.

2.2.2 PVDF-based solid electrolytes. The –CF group of PVDF (polyvinylidene fluoride) makes it have a high dielectric constant and strong electron absorption characteristics, and the rigidity and chemical resistance of the PVDF chain segment ensures good mechanical properties and chemical stability.[38] However, its ionic conductivity remains low compared with other materials (such as gel electrolytes), its crystallinity is high, and it is brittle and has poor toughness.[39] *N*,*N*-Dimethylformamide (DMF) is a common solvent and plasticizer for the preparation of PVDF based electrolytes. The residual DMF solvent can form $[Li(DMF)_x]^+$ with Li^+, which conducts Li^+ by coordination/unpairing with fluorine atoms on the PVDF chain.[40,41] Xu *et al.* used lipophilic lithium magnesium silicate (LLS) to refine polymer particles, which can promote ion transport while reducing crystallinity and stabilizing interface, and the ionic conductivity is 2.07×10^{-4} S cm^{-1} at 30 °C.[42]

Single-phase SPEs cannot meet the needs of high-performance solid-state batteries. The emergence of organic–inorganic composite solid-state polymer electrolytes may combine the advantages of both types, potentially breaking existing limitations and serving as a key to advancing solid-state battery development (Fig. 3 and Table 1).

2.3 Organic–inorganic composite solid polymer electrolytes (CSPEs)

CSPEs are composed of polymers, lithium salts and fillers, combining the benefits of SPEs and ISEs. However, they also face serious interface problems.[46] The physical and chemical properties of organic phase and inorganic phase are different, so that the two are prone to phase separation, and some inorganic materials have high chemical activity on the surface, prone to side reactions, with the side reaction products covering the surface of the electrode or filling the interface between the electrolyte and the electrode, which will lead to increased interface impedance.[47–50] Jin *et al.* used the "multi-affinity" of the 12C4-TFSI supramolecular nanomodification layer to connect PVDF, LLZTO and LiTFSI, and realized the interface optimization among the components in CSPEs.[51] Wu *et al.* used PAA with a small LUMO–HOMO gap to remove alkaline impurities such as Li_2CO_3, reduce the degree of dehydrofluorination of PVDF, and improve the compatibility with polymer matrix.[52]

In addition, a layer of material with good compatibility and ionic conductivity is inserted at the interface as the interface buffer layer, which can improve the interface contact condition

Table 1 Comparison of the characteristics of different solid electrolytes and their compatibility with anode materials

Classification	Advantages	Disadvantages	Matching issue with anode (such as lithium metal)
Oxide	High-pressure resistance (4–5 V)	High rigidity and poor interface contact	Poor infiltration with lithium metal
	Good stability and low cost	Low ionic conductivity (10^{-4} to 10^{-3} S cm^{-1})	Interface side reaction may result in the formation of a high-resistance layer
Sulfide	High ionic conductivity (10^{-3} to 10^{-2} S cm^{-1})	Sensitive to air and generates H_2S when in contact with water	Poor interface stability with lithium metal, prone to form lithium dendrites
	Good extensibility, easy to be processed into films	Low oxidation potential (easily reacts with the positive electrode at high voltage)	
Halide	High ionic conductivity (10^{-3} S cm^{-1}) and superior air stability compared with sulfides	High cost of raw materials	Poor infiltration of lithium metal
	Combining the advantages of sulfides and oxides	Low reduction potential, poor compatibility with lithium metal	Interface side effect
Polymer	Good flexibility	Low ionic conductivity (10^{-7} to 10^{-5} S cm^{-1})	Insufficient mechanical strength, lithium dendrites are prone to penetrate
	Good interface contact	Poor ability to withstand high pressure (<4 V)	

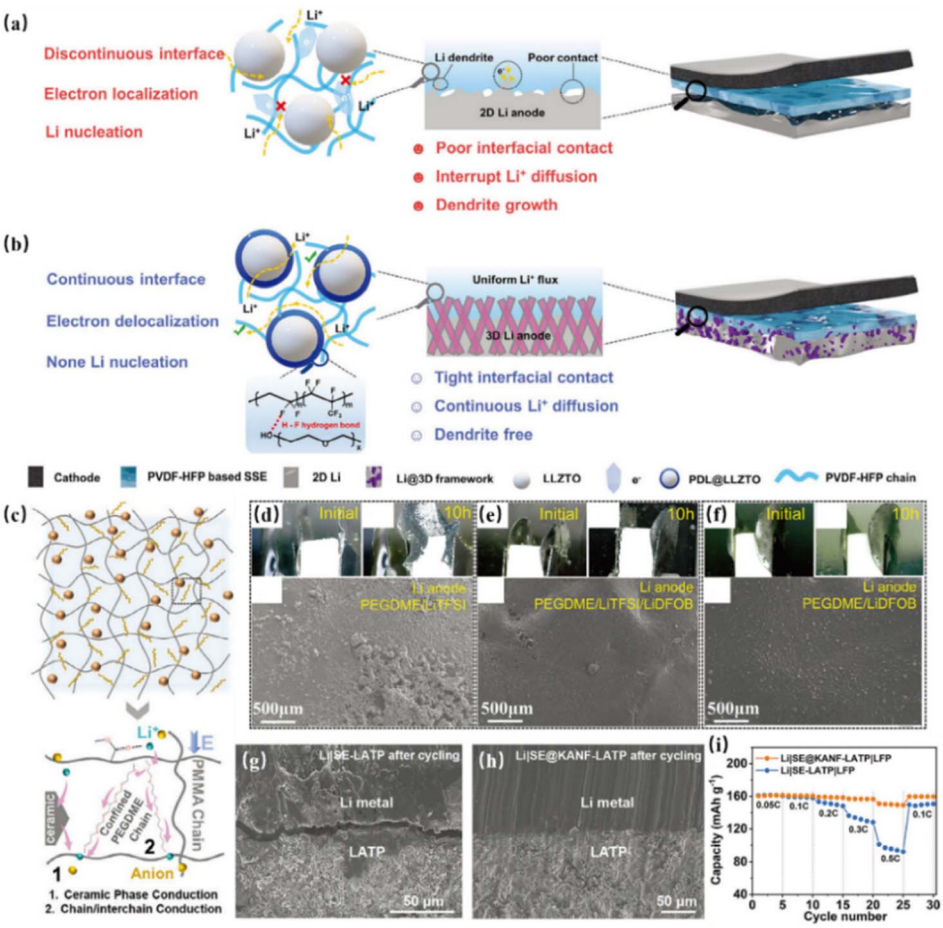

Fig. 4 (a) Schematic of Li^+ transport and charge distribution at the electrolyte–electrode interface in LLZTO and (b) PDL@LLZTO effect of electrolyte on 2D/3D lithium anodes.[57] (c) Diagram of the PEGDME@PMMA electrolyte and internal Li^+ transport.[54] Digital photos and SEM of lithium deposition before cycling and after 10 hours for (d) PEGDME/LiTFSI, (e) PEGDME/LiTFSI/LiDFOB, and (f) PEGDME/LiDFOB.[54] SEM of cross-sections after cycling of (g) Li|SE-LATP and (h) Li|SE@KANF-LATP.[53] (i) Performance of Li|SE@KANF-LATP|LFP and Li|SE-LATP|LFP.[53]

and effectively avoid the interface side reaction. Wang *et al.* coated nano-porous KANF on the LATP surface and constructed a SE@KANF protective layer by *in situ* polymerization, which could improve the interface stability of the effective lithium anode.[53] Wang *et al.* improved the mechanical properties of the electrolyte by *in situ* polymerization of low molecular weight polyethylene glycol dimethyl ether (PEGDME) and polymethyl methacrylate (PMMA). Lithium difluoro (oxalate) borate (LiDFOB) forms a fluorine-rich SEI film at the lithium anode interface, effectively restraining the side reaction and improving the interface stability.[54]

In several mainstream solid electrolytes, the movement of polymer chain segments in polymer solid electrolytes is relatively limited under RT, resulting in a slow Li^+ migration rate.[55] The oxide-based solid electrolyte has a relatively stable crystal structure framework and a suitable Li^+ transmission channel. Some electrolytes can achieve ionic conductivity of about 10^{-4} S cm^{-1} under RT. However, issues related to interface compatibility remain difficult to resolve.[56] Sulfide-based solid electrolytes achieve ionic conductivities of 10^{-3} S cm^{-1} or higher at RT due to their relatively low ion migration energy barriers and loose structures. However, significant side reactions present urgent challenges. The composite electrolyte has high ionic conductivity, good thermal stability and mechanical properties, which can promote the rapid development of solid-state battery applications. Solving problems such as oxide interface impedance and sulfide side reactions will promote the medium-and long-term application of solid-state batteries (Fig. 4).

3. Anode of solid-state batteries

Anode materials in solid-state batteries are critical for energy storage and release, significantly influencing energy density, stability, and compatibility with solid electrolytes. It is essential for anode materials to maintain a stable interface with solid electrolytes to ensure battery efficiency and longevity.[58] Traditional graphite anodes have struggled to meet the needs of high energy density solid-state batteries, leading to a shift towards high-performance anode materials such as silicon, lithium, and even anode-free designs. Lithium metal and silicon-based anodes have extremely high specific capacities and are becoming prime candidates for next-generation solid-state batteries. It is expected that silicon-based anodes will first be applied to polymer and polymer oxide solid-state batteries, followed by the integration of silicon and lithium in pure oxide or sulfide systems, with the ultimate goal of high-performance solid-state batteries with lithium anodes or no anodes at all. The lithium metal anode provides the lithium source directly to the battery, significantly increasing the energy density and reducing the charging time. However, they still face challenges such as lithium dendrite formation, unstable and uneven interface contact, unstable solid electrolyte interphase (SEI) films, and low critical current density (CCD).[59] Silicon has the

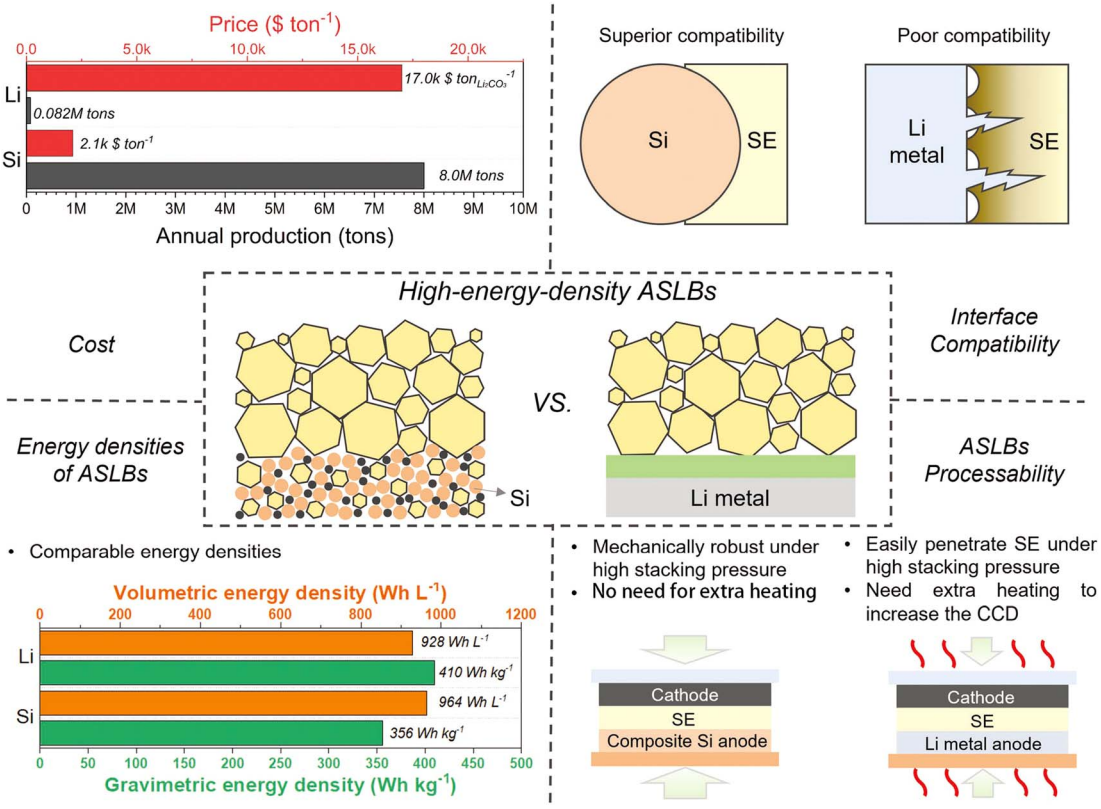

Fig. 5 Comparison of silicon anodes and lithium metal anodes in all-solid-state lithium batteries.[63]

advantages of large theoretical capacity and abundant availability. The risk of forming lithium dendrites is low due to good alloy reaction kinetics and high lithium deimpingement potential. However, significant volume expansion, irreversible side reactions at the interface, and poor intrinsic conductivity severely hinder its practical application.[60] Achieving dense contact between the solid electrolyte and anode materials not only reduces interfacial resistance and ensures smooth Li^+ transport between the anode and electrolyte but also effectively suppresses lithium dendrite formation, thereby enhancing the cycling stability and safety of the battery.[61,62] However, most solid electrolytes are difficult to wet and permeate porous electrodes, with side reactions further exacerbating interface problems (Fig. 5).

In solid-state batteries, anode materials store and release energy through repeated Li^+ insertion and deinsertion. The solid electrolyte isolates the anode from the cathode to prevent short circuits, while providing high ionic conductivity and good chemical stability, ensuring efficient Li^+ transfer between the anode and cathode. During the charge and discharge process, Li^+ migrates through the solid electrolyte, and a redox reaction occurs to promote the storage and release of energy. The close contact between the solid electrolyte and the negative electrode material reduces the interface resistance, ensures the smooth transfer of Li^+, effectively inhibits the growth of lithium dendrites, and improves the stability and safety of the cycle.[61,62,64] But, most SSEs are difficult to wet and permeate porous electrodes, resulting in poor electrolyte–electrode interface contact. However, because of their minimal interfacial side reactions, they are compatible with lithium metal and silicon-based anodes, offering the potential to overcome the energy density limitations of commercial lithium batteries.

3.1 Interface issues of silicon-based anodes

Silicon has a theoretical capacity of about 3600 mA h g^{-1} (nine times that of graphite), is abundant, environmentally friendly, and has a suitable electrode potential (0.4 V *vs.* Li/Li^+), which effectively prevents lithium deposition and dendrite growth, solving key problems related to the anode.[65] However, due to the volumetric expansion effect, silicon-based anode materials often

Table 2 Electrochemical performance of silicon-based anodes in various solid-state electrolytes

Anode	SE	Ionic conductivity/S cm^{-1}	Current density	Capacity/mAh g^{-1}	Ref.
Si–N-MXene	PEO@LATP	3.4×10^{-4}/50 °C	0.4 A g^{-1}/50 °C	First: 2305 10th: 1362	70
Si@SiO_2@LPO@C	PEO/LATP	2.86×10^{-5}/50 °C	0.2 A g^{-1}/50 °C 0.5 A g^{-1}/50 °C	First: 2482 First: 2279 20th: 1001	71
Si@MOF	PVDF/PEO/LLZTO	8.1×10^{-5}/25 °C	200 mA g^{-1}/60 °C	First: 1416	72
Si	LLZAO	4×10^{-4}/RT	0.66 mA h cm^{-2}	First: 2685	73
Si@Li_6PS_5Cl	Li_6PS_5Cl	—	0.1 mA cm^{-2}	First: 2412	74
Si@LPSCl	$Li_{5.4}PS_{4.4}Cl_{1.6}$	$\sim 8 \times 10^{-3}$/RT	0.2–0.5 mA cm^{-2}/RT	First: 2412 50th: 1136	75
Si/CNTs/C/Li_6PS_5Cl	Li_6PS_5Cl	2.13×10^{-3}/RT	50 mA g^{-1}	50th: 1226	76

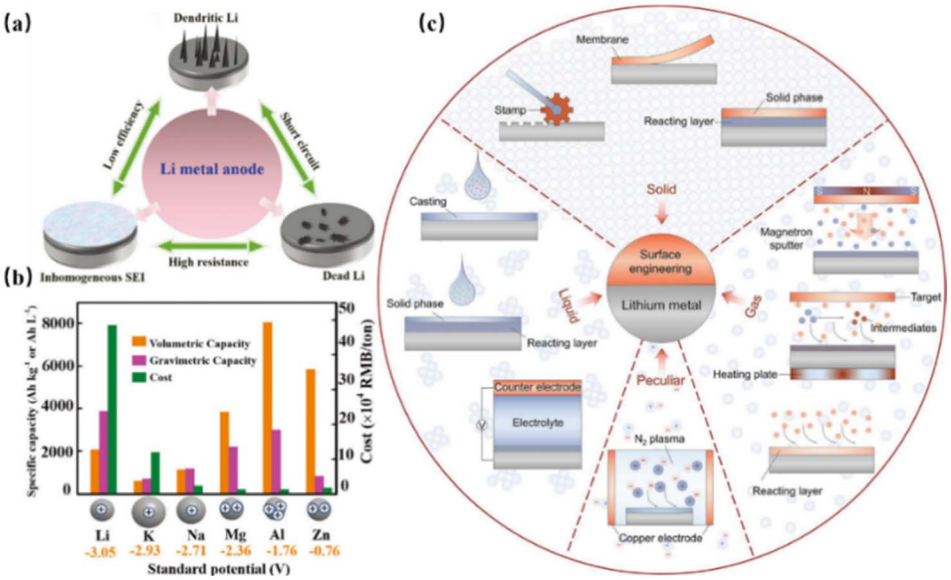

Fig. 6 (a) and (b) Characteristics of lithium anodes;[82] (c) strategies for improving interfacial issues.[83]

experience particle breakage and continuous solid–electrolyte interface (SEI) formation, leading to lithium loss and rapid capacity decline. Unlike liquid batteries, the mechanical rigidity and external stacking pressure of the solid electrolyte in solid-state batteries reduce or alter SEI formation and particle breakage in silicon-based anodes, potentially improving cycle stability.[66,67] In all-solid-state batteries, the low mobility of silicon SEI films makes inorganic solid-state silicon anodes an effective method to reduce the side reactions at the electrode–electrolyte interface. Although the formation of a less mobile SEI in solid-state silicon anodes can slow down the repeated growth of interfacial phases and enhance cycling life, it may also lead to a lower initial coulombic efficiency (ICE) (Table 2).[68,69]

3.2 Interface issues of lithium metal anodes

Lithium metal anode has a high theoretical specific capacity (3860 mA h g^{-1}), low electrode potential and low density, and is considered to be the ideal anode material for high-performance solid-state batteries. However, issues such as lithium dendrite formation, poor physical contact, and poor interfacial compatibility significantly hinder their application.[77,78]

SSEs will inevitably be spontaneously reduced by the lithium metal, resulting in the formation of unstable SEI on the surface of the lithium metal anode. In addition, the rigid contact between the electrolyte and the anode causes ions and electrons to be unevenly distributed at the interface, hindering the transfer of ions and electrons.[79] In addition, the volume change of lithium metal during the cycle causes the electrolyte–anode interface to lose contact, reducing ion transport pathways. Moreover, the high reactivity of lithium metal will produce side reactions when in contact with solid electrolyte, which will not only consume active lithium, increase interface resistance, hinder the transmission of lithium ions, but also lead to uneven Li^+ flux and local high current density which promotes the growth of lithium dendrites, thereby penetrating the electrolyte layer and causing short circuit.[80,81] In recent years, the RT ionic conductivity of solid-state batteries has been significantly improved, transforming the performance bottleneck of solid-state batteries from the problem of low ionic conductivity to the problem of electrolyte–electrode interface compatibility (Fig. 6).

4. Interface mechanism issues between solid-state electrolytes and anodes

The ideal SSEs-anode interface should exhibit low interfacial resistance, close contact, and excellent electrochemical/

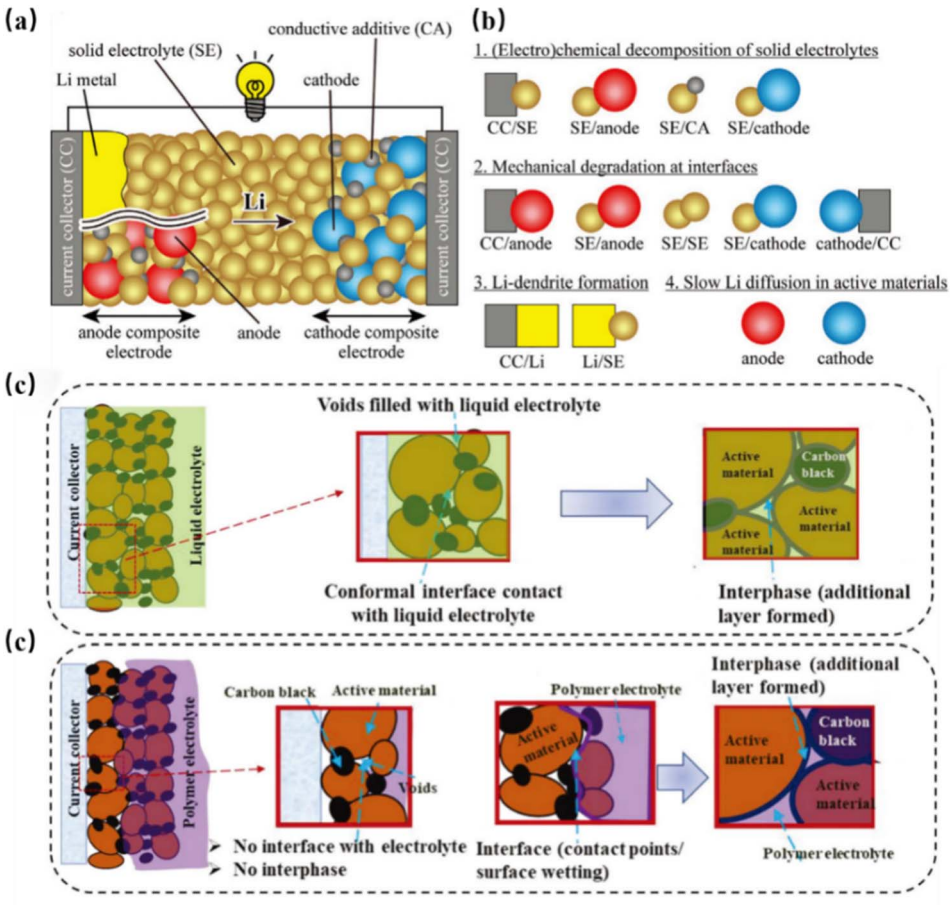

Fig. 7 (a) Configuration of ASSBs and (b) key issues at the solid electrolyte–electrode interface.[86] Schematic of the electrolyte–electrode interface in (c) liquid and (d) solid batteries.[82]

mechanical stability. However, due to the complex interaction between the SSE and anode, as well as their mismatch in physical, chemical, and electrochemical properties, the solid–solid contact interface has poor contact, compatibility issues, and unstable ion transport, which seriously hinders the performance improvement and commercialization of solid-state batteries.[62,84] The interfacial instability between SSEs and anodes is a primary cause of performance degradation in solid-state batteries. Although interfacial electrochemical reactions and dendrite growth both contribute to the transport of lithium ions, the mechanisms for the formation of gaps at the interface of lithium metal and silicon-based anodes are fundamentally different. Therefore, it is necessary to study each of these mechanisms and their effects in depth (Fig. 7).[85]

4.1 Growth of lithium dendrites

Lithium dendrites pose a serious challenge to lithium metal anodes. Although SSEs have many advantages over LEs, they have difficulty in uniformly conducting Li^+, resulting in local concentrations of Li^+ and promoting dendrite growth in specific areas.[87,88] Nagao *et al.* characterized the growth of lithium along grain boundaries using *in situ* scanning electron microscopy and found that dendrite growth induced local stress and electron accumulation, leading to the formation of cracks. This leads to the continuous accumulation and growth of dendrites at grain boundaries and cracks, which eventually punctures the electrolyte film, causing short circuits and thermal runaway.[89] The growth of lithium dendrites is a complex electrochemical process influenced by many factors such as ionic diffusion, overpotential, concentration gradients, and mechanical stress.[90] Harry *et al.* found that the random distribution of irregular impurities, such as Li_2O or LiOH, leads to uneven lithium deposition and dendrite growth.[90] Current density is also a crucial factor affecting dendrite growth. Due to the low Li^+ mobility in some SSEs, the high current density creates a cation concentration gradient on the surface of the lithium metal anode, further exacerbating dendrite growth.[91] Near the SSS-lithium anode interface, the uneven distribution of local ion transport paths, crystal defects, ion concentration, current, overpotential and stress are important factors that trigger and aggravate the formation of lithium dendrites. Future systematic studies should focus on these factors within specific solid electrolyte systems to clarify the underlying mechanisms and guide the design of electrolyte–anode interfaces (Fig. 8).

4.2 Volume effect exacerbates interfacial impedance

On the one hand, the solid–solid interface between the solid electrolyte and anode features a small contact area, poor physical contact, and inadequate interface stability (*e.g.*, due to byproducts from interfacial side reactions), which can increase charge transfer resistance and hinder effective Li^+ transport. In solid-state batteries, the combined effect of anode volume and lithium dendrite growth significantly changes the interface structure, further disrupting the existing ion conduction pathway and increasing the interface resistance. On the other hand, high-performance anode materials like silicon and lithium typically experience significant volume expansion and contraction during cycling. The rigid contact interface between the SSE and anode is particularly sensitive to these volume changes, resulting in interface contact degradation, potential crack formation, and the creation of large stresses that can directly break the interface. In addition, the interfacial side

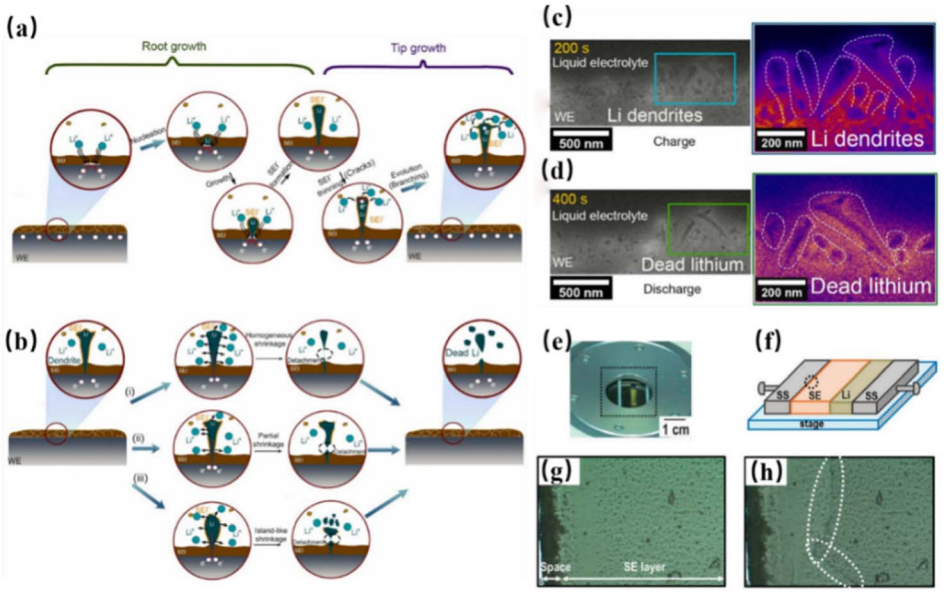

Fig. 8 Schematics of lithium dendrite growth and dissolution dynamics during (a) charging and (b) discharging;[92] ADF-STEM images showing dendrite growth at the interface (c) after 200 s and (d) 400 s of cycling.[87] (e) Photo of *in situ* optical microscope viewing device and (f) measurement schematic, highlighting morphological changes at the dashed circle. (g) Optical microscopy images of the SSE-SS interface before testing and (h) after lithium deposition for 730 s at 2 mA cm^{-2}.[93]

reaction alters the stress distribution at the electrolyte–anode interface, leading to continuous degradation and hindering ion transport across the interface.[94] Liu *et al.* used a multi-physics simulation method to monitor the change of stress distribution at the interface between $Li_{1.3}Al_{0.3}Ge_{1.7}(PO_4)_3$ (LAGP) and lithium metal anode. Their results confirm that lithium metal electrodeposition causes interfacial compression and stress concentration, disrupting the interfacial balance and leading to a rapid decline in battery performance.[95] Cao *et al.* constructed a continuous, crack-free MgF_2 nanoscale film on the surface of garnet-type solid electrolyte $Li_{6.5}La_3Zr_{1.5}Ta_{0.5}O_{12}$ (LLZTO). This resulted in a significant reduction in the LLZTO–lithium anode interfacial impedance from 1190 Ω cm^2 to 6 Ω cm^2, effectively suppressing lithium dendrite formation and ensuring stable battery cycling.[96] Zhang *et al.* introduced polystyrene sulfonate lithium (PLSS) to the surface of LLZTO and used the $-SO_3Li$ group to bind to metal elements on LLZTO. This effectively reduces the Li^+ migration activation energy, increases the Li^+ diffusion coefficient, inhibits the growth of lithium dendrites, and achieves a stable cycle, so that the interface impedance of Li/LLZTO–PLSS/Li is significantly reduced to 9 Ω cm^2, and the critical current density is increased to 1.1 mA cm^{-2}.[97]

4.3 Stress–strain and electronic structure affect interfacial impedance

In addition, due to the differences in surface roughness and crystal structure between solid electrolyte and anode material, it is difficult to achieve tight and uniform contact when the two are assembled into batteries, hindering effective ion transport at the interface. With the generation and gradual accumulation of structural stress at the interface during charge and discharge cycle, interface superlattice, stress strain and structural defects occur. This further hinders ion transport, resulting in a continuous increase in interface impedance.[95] The energy level corresponding to the highest occupied molecular orbital (HOMO) and the lowest unoccupied molecular orbital (LUMO) between the electrolyte and the anode plays a decisive role in the chemical stability of the interface. For example, the anodic reduction of $Li_{0.33}La_{0.56}TiO_3$ (LLTO) and $Li_{1.3}Al_{0.3}Ti_{1.7}(PO_4)_3$ (LATP) occurs at 1.7 V and 2.4 V, respectively. The reduction of Ti^{4+} to Ti^{3+}, which is unstable to lithium metal, limits the electrochemical stability window, forms cracks between adjacent ion channels and increases grain boundary resistance (Fig. 9).[98,99]

4.4 Side reactions at the interface reduce energy density and increase impedance

Under the dual drive of electrochemical and chemical processes, side reactions occur at the electrolyte–anode interface and form by-products, resulting in increased interface impedance, which is a major key problem of solid-state batteries. On the one hand, the electronic conductivity of amorphous mixed ionic intermediates in these side reactions perpetuates irreversible reactions, leading to continuous decomposition of the electrolyte and worsening of lithium metal's non-uniform growth. This further intensifies interfacial degradation, leading to irreversible loss of the by-product Li^+, ultimately reducing the coulombic efficiency and energy density of the battery.[102] On the other hand, the poor ionic conductivity of the byproducts from interfacial side reactions can hinder ionic transport at the interface, increasing interfacial impedance and reducing the battery's power density, capacity, and lifespan. Due to the high electrochemical reactivity of lithium metal anodes, almost all solid electrolytes are thermodynamically unstable to them, except for common by-products such as LiF, Li_3N, and Li_2O.[8,103,104] By-products often have a negative impact on battery performance. For example, the side reaction between lithium and the PEO electrolyte produces Li_2O, C_2H_4 and H_2, which not only breaks the close contact between the electrolyte and anode interface, but also hinders the transmission of Li^+ due to the low ionic conductivity of Li_2O.[105] The accumulation of gas generated by side reactions at the internal interface of the battery cannot be discharged, resulting in increased internal stress and battery

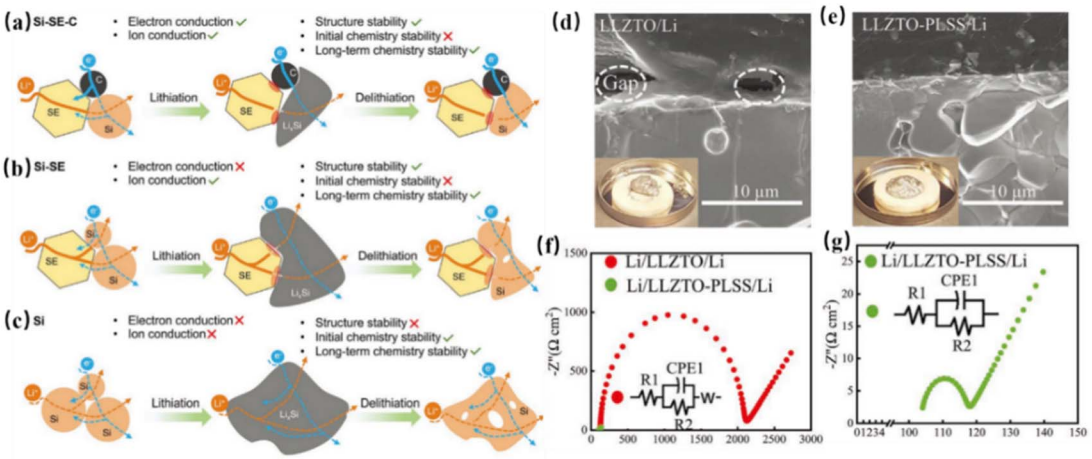

Fig. 9 Schematic of the chemical and structural evolution of (a) Si-SE-C, (b) Si-SE, and (c) Si anodes in all-solid-state batteries;[100] SEM of (d) LLZTO/Li and (e) LLZTO–PLSS/Li;[101] EIS for (f) Li/LLZTO/Li and (g) Li/LLZTO–PLSS/Li.[101]

expansion, compromising structural integrity and increasing the risk of safety accidents.

5. Effective measures to mitigate interface issues

5.1 First-principles and artificial intelligence computing guide the design of materials and charge–discharge processes

First-principles and artificial intelligence calculations are powerful tools for predicting the (electro)chemical stability of electrolyte–electrode interfaces. Huang *et al.* investigated the thermodynamic stability between silicon and sulfide-SSEs, revealing that the reactions are primarily driven by interactions between Si and P, resulting in the formation of SiP_2, SiP, and Li_5SiP_3. The electrode potential of SiP_2, SiP (1.5 to 0.97 V *vs.* Li^+/Li) and Li_5SiP^3 (0.96 to 0.76 V *vs.* Li^+/Li) is significantly higher than that of silicon, resulting in a lack of reversibility in the operating voltage range of silicon, which increases the anode potential, internal resistance, and reduces the coulombic efficiency.[106] In the field of solid-state battery research, effectively screening and designing materials suitable for battery interfaces remains a critical challenge for scientists. However, traditional material screening methods often rely on extensive experimentation and high computational costs, resulting in lengthy development cycles and low efficiency. Li *et al.* proposed a material screening framework based on transfer learning that integrates crystallogram convolutional neural networks to train highly predictive models using limited data. The method successfully identified 12 promising SEI materials, breaking the traditional reliance on large data sets and providing a viable way to rapidly screen materials in solid-state batteries, demonstrating the great potential of artificial intelligence in guiding material design.[107] Xu *et al.* developed a systematic Ge atom substitution screening process to solve the interface problem of $Li_{10}GeP_2S_{12}$. This process led to the identification of a new solid electrolyte, $Li_{10}SrP_2S_{12}$. The results show that the LSrPS–Li interface has a larger Schottky barrier (0.13 eV), smaller electron transfer region (3.10 Å), and a stronger ability to block excess electrons. Replacing Ge with Sr improves the stability of the battery interface without affecting the lithium-ion conductivity of the LGPS.[108]

5.2 Optimizing the electrochemical window

The interaction and compatibility between solid electrolytes and anode materials are crucial for the performance of solid-state batteries. Poor interface compatibility can lead to issues such as internal cracking, hindered ionic transport, and increased battery impedance. Enhanced interface compatibility optimizes the SSE-anode interaction, thereby improving the stability and efficiency of the battery.

The electrochemical stability window of an electrolyte reflects its ability to resist undesirable electron transfer and is a key parameter for evaluating the compatibility of solid electrolyte–anode interface. Both CV tests and DFT calculations can determine the electrochemical window, but their results often show significant differences. For example, the calculated electrochemical window of Li_6PS_5Cl is only 1.71–2.01 V, while its measured value can reach 7 V.[109,110] Due to the high reactivity of lithium metal anodes, most electrolytes are unstable in their presence. The formation of an interface phase with high ion conductivity and low electron transport capacity can act as a passivation layer, hindering the continuous decomposition of the electrolyte–lithium metal anode interface, thus expanding the electrochemical window.

5.3 Suppressing lithium dendrite growth

The growth of lithium dendrites is influenced by various factors, including the intrinsic characteristics of the electrolyte, temperature, lithium deposition rate, and electrode surface conditions. Incomplete dissolution of dendrites during cycling can lead to the formation of dead lithium, causing loss of electrical contact with the current collector upon stripping. Furthermore, dendrite growth may penetrate solid electrolytes, resulting in internal short circuits, capacity degradation, and thermal runaway risks. Therefore, suppressing lithium dendrite growth is crucial for addressing interfacial issues between solid electrolytes and electrodes. Liu *et al.* utilized magnetron sputtering to construct an electromechanical buffering layer on the LATP surface through the spontaneous reaction between metallic lithium and Ti–LiF films. This approach facilitated uniform and effective Li^+ migration across the interface while dissipating interfacial stress generated during lithium growth.[111] Sun *et al.* inhibited the growth of lithium dendrites by introducing an interfacial layer doped fluorocarbon phosphate (FA). The inherent electrostatic shielding and self-healing properties of Cs reduce the nucleation potential of lithium ions and the binding energy of LiTFSI, promote the uniform deposition of Li^+, and enhance the stability of the lithium metal surface.[112] Xie *et al.* used $Sn(Oct)_2$ to initiate *in situ* ring-opening polymerization of ε-caprolactone (ε-CL), forming LiSn mesophase layer at the anode interface and inhibiting the growth of lithium dendrites. At a current density of 0.05 mA h cm^{-2}, the assembled symmetric battery can be stably cycled for 900 h, while the non-*in situ* polyelectrolyte battery shorted out after only 200 h.[113] Wang *et al.* constructed a Li/LLZO interface *in situ* that could be observed from the cross-sectional direction in TEM. Through phase field simulation and molecular dynamics calculations, they clarified the mechanism of the interface pores causing local electric field concentration and the difference in lithium atom diffusion rate, providing theoretical guidance for interface optimization.[114]

5.4 Controlling volume effects in anode materials

Controlling the volume effect of the anode material is essential to maintain the stability of the electrolyte–anode interface and ensure electrochemical performance. For example, active materials such as lithium metal and silicon-based anodes experience significant volume fluctuations during cycling, leading to interface contact failure and electrolyte structure destruction, resulting in increased interface impedance and blocked Li^+ transport pathways. Ci *et al.* introduced a $LiAlO_2$ coating with high ionic conductivity and mechanical strength

on the Si surface, which not only facilitates Li^+ transfer at the interface but also mitigates silicon's volume expansion, thereby preserving the electrode structure and the electrolyte–silicon anode interface.[115] Zhang *et al.* developed a Si@MOF anode by embedding nano-silicon into MOF-derived carbon matrix, which effectively alleviated the volume expansion of silicon. The assembled LFP/PVDF-PEO-LLZTO/Si@MOF full battery has an initial capacity of 135 mA h g^{-1} and a capacity retention rate of 73.1% after 500 cycles at 0.5C and 60 °C.[116]

5.5 Enhancing interfacial wettability

The effective contact area between the electrolyte and anode in solid-state batteries primarily depends on their interfacial wettability. For example, LLZO exhibits high contact angles, resulting in elevated apparent interface resistance. However, rapid acid treatment and *in situ* shielding can produce Li_2CO_3-free lithium wettable LLZO, which reduces interfacial resistance.[117,118] The side reaction between electrolyte and electrode can change the interface properties, thus affecting the wettability. Certain composite coatings can simultaneously provide rapid Li^+ diffusion pathways, high modulus, and shape consistency. For example, films composed of PVDF-HFP mixed with rigid LiF particles can enhance interfacial ion conductivity and physical/chemical stability when used as an artificial SEI on lithium metal anodes.[119] Cao *et al.* assembled a high-voltage bipolar stacked all-solid-state battery using NCM811, Li_6PS_5Cl, and Si, employing ethyl cellulose as a binder due to its amphiphilic nature and strong adhesion. This approach achieved good compatibility with sulfide solid electrolytes and high thermal stability.[74] Yan *et al.* synthesized a stable lithium–silicon alloy anode with hard carbon, consisting of a deformable lithium-rich phase ($Li_{15}Si_4$ and LiC_6) to form a three-dimensional ion/electron conducting network. This structure increases the active surface area, reduces stress concentration, and optimizes interface contact.[120] *In situ* synthesis technology makes the contact between the solid electrolyte and the anode material uniform and dense, improves the mechanical strength and stability of the interface, and realizes the good compatibility between the two components.

5.6 Suppressing of interfacial side reactions

Interface side reactions can lead to increased internal resistance, reduced capacity, shortened life, and even safety issues. Therefore, inhibiting these side reactions is crucial to improving battery performance. Utilizing materials such as PPF_{40},[121] lithium polymer in F diluents,[122] ionic liquids,[123] Cu_3P,[124] graphene,[125] Li_3OCl,[126] aluminosilicate,[127] Mo_6S_8/C@Li,[128] and clay/cross-linked network polymers[129] as interfacial buffer coatings can significantly improve the contact interface between the electrolyte and electrode, thereby reducing interfacial side reactions. By using molecular layer deposition technology, Sun *et al.* prepared an inorganic–organic composite coating at the interface of silicon anode and sulfide solid electrolyte, which significantly reduced the side reactions at the interface.[130] Hyeon *et al.* effectively suppressed interfacial side reactions and promoted ion migration and uniform reactions by coating Li_6PS_5Cl solid electrolyte on two-dimensional conductive graphene-like carbon (GLC@LPSCl), resulting in approximately 90% capacity retention after 200 cycles.[131] Kaskel *et al.* constructed a cylindrical silicon anode structure-Li_6PS_5Cl 2D transverse SEI, which combined with mechanical stability under external pressure reduced the surface area of the side reaction, and the copper dendrites on the fluid collection ensured good electrical conductivity and adhesion of active substances along the direction of the column.[68] In addition, electrolyte additives can form a stable protective film at the interface, promote Li^+ migration, inhibit interface side reactions, and enhance the chemical stability of the interface.[132–134]

In summary, in the optimization of the interface between solid-state electrolytes and anode materials, multiple strategies exhibit complementarity and limitations. Computational-guided design accelerates material development through atomic-level mechanism prediction and high-throughput screening, but is limited by computational resource consumption and the accuracy of dynamic process modeling (such as the multi-scale evolution of lithium dendrite growth). In terms of electrolyte modification, doping technology can enhance the electrochemical window of sulfides, but is limited by its inherent voltage tolerance and requires combined composite material design to balance its performance and process feasibility. In interface engineering, high mechanical strength electrolytes can inhibit lithium dendrite growth, but rigid interfaces are prone to contact failure; ionic liquids or polymer coatings can improve wettability, but may introduce thermal stability risks. In negative electrode optimization, although nanoscale or pre-lithiation treatment of silicon-carbon anodes can alleviate volume effects, it sacrifices energy density and cycle life. The control of side reactions relies on the construction of stable SEI membranes, but the dynamic evolution mechanism still lacks precise control means. Currently, semi-solid batteries have achieved preliminary commercialization through compromise solutions, while the all-solid-state system still needs to break through interface impedance and process bottlenecks. In the future, it is necessary to integrate collaborative strategies such as AI simulation-guided material design, *in situ* characterization dynamic monitoring, and multi-dimensional interface regulation to promote the industrialization process.

6. Summary and outlook

This paper reviews the recent progress of solid electrolyte–anode interface problems and optimization strategies to promote the development of high-performance sensors. At present, the solid electrolyte–anode interface faces the following challenges: (a) uneven lithium deposition leads to the growth of dendrites, which can penetrate the electrolyte, leading to short circuits and thermal runaway; (b) bad contact leads to high interface impedance, and the volume effect and stress changes during charge and discharge lead to interface degradation, which limits ion transport and reduces capacity; (c) serious interfacial side reactions lead to lithium loss, deterioration of interfacial contact, limited ion transport and gas

production expansion, resulting in decreased energy density and damage to the overall structure of the battery.

In response to these interface problems, researchers have tried a series of strategies to alleviate the interface problems, but the side reactions and interface contact impedance problems have not been completely solved. In the future, the following research ideas may be used to promote the application of all-solid-state lithium batteries: (a) employing advanced *in situ* characterization techniques and simulation calculations to gain a deeper understanding of the electrochemical behavior at the solid electrolyte–anode interface; (b) investigating the effects of charge–discharge parameters on the evolution of the electrolyte–anode interface; (c) improving interfacial stability through the construction of interfacial transition layers, modification of electrolyte and anode materials, and optimizing interfacial fabrication processes.

Solid electrolyte–anode interface with good physical contact, high ionic conductivity, stable (electrical) chemical stability and excellent self-healing ability is crucial to improve the high energy density and high safety of all-solid-state lithium batteries. The solution of this problem will strongly promote the large-scale practical application of high-performance all-solid-state lithium batteries and greatly accelerate the arrival of the era of comprehensive electrification in the field of energy transportation.

Data availability

Data will be made available upon request.

Author contributions

Dandan Wang: conceptualization, methodology, and writing-original draft. Xinyang Wu: investigation and methodology. Yongpeng Ren: conceptualization, funding acquisition, and writing-review & editing. Yaru Li: conceptualization, funding acquisition, and writing-review & editing. Xiaolin Xie: investigation, formal analysis, and funding acquisition. Xiqiang Ma: investigation, formal analysis, and funding acquisition. Xuemin Chen: investigation. Junhao Lu: investigation. Kunming Pan: funding acquisition, project administration, and supervision.

Conflicts of interest

The authors declare that they have no known competing financial interests or personal relationship that could have appeared to influence the work reported in this paper.

Acknowledgements

This work was supported by Frontier exploration Projects of Longmen Laboratory (LMQYTSKT012 and LMQYTSKT037), Major Scientific and Technological Innovation Project in Henan Province (231100220100), Youth Project of Henan Natural Science Foundation (222300420134), the Key Research and Development Project of Henan Province (No. 241111231600), Major Science and Technology Projects of Longmen Laboratory (ZDYF-001), the Longmen Laboratory "Trendy Industry Projects" (LMFKCY2023002), and Longmen laboratory concept verification project (GNYZ-202501).

References

1 D. Razzaghi, M. Babazadeh-Mamaqani, A. Babaie, F. Esmati, H. Roghani-Mamaqani, M. Rezaei, K. De Clerck and R. Hoogenboom, *ACS Appl. Mater. Interfaces*, 2025, **17**, 4247–4289.
2 R. Götz, R. Streng, J. Sterzinger, T. Steeger, M. M. Kaye, M. Vitort and A. S. Bandarenka, *InfoMat*, 2024, **6**, e12627.
3 J. Wu, M. Zheng, T. Liu, Y. Wang, Y. Liu, J. Nai, L. Zhang, S. Zhang and X. Tao, *Energy Storage Mater.*, 2023, **54**, 120–134.
4 B. B. Gicha, L. T. Tufa, N. Nwaji, X. Hu and J. Lee, *Nano-Micro Lett.*, 2024, **16**, 172.
5 T. Schmaltz, F. Hartmann, T. Wicke, L. Weymann, C. Neef and J. Janek, *Adv. Energy Mater.*, 2023, **13**, 2301886.
6 M. Wan, S. Kang, L. Wang, H. W. Lee, G. W. Zheng, Y. Cui and Y. Sun, *Nat. Commun.*, 2020, **11**, 829.
7 M. Liu, A. Song, X. Zhang, J. Wang, Y. Fan, G. Wang, H. Tian, Z. Ma and G. Shao, *Nano Energy*, 2025, **136**, 110749.
8 Y. Zheng, S. Zhang, J. Ma, F. Sun, M. Osenberg, A. Hilger, H. Markter, F. Wilde, I. Manke and Z. Hu, *Sci. Bull.*, 2023, **68**, 13.
9 J. Kim, G. Yoon, S. Kim, S. Sugata, N. Yashiro, S. Suzuki, M. Lee, R. Kim, M. Badding, Z. Song, J. Chang and D. Im, *Nat. Commun.*, 2023, **14**, 782.
10 K. Shen, W. Shi, H. Song, C. Zheng, Y. Yan, X. Hong, X. Liu, Y. An, Y. Li, F. Ye, M. He, G. Ye, C. Ma, L. Zheng, P. Gao and Q. Pang, *Adv. Mater.*, 2025, **37**, 2417171.
11 E. P. Alsaç, D. L. Nelson, S. G. Yoon, K. A. Cavallaro, C. Wang, S. E. Sandoval, U. D. Eze, W. J. Jeong and M. T. McDowell, *Chem. Rev.*, 2025, **125**, 2009–2119.
12 X. Wang, D. Guan, X. Ma, X. Yuan, Q. Zhu, H. Deng, H. Wang and J. Xu, *Angew. Chem., Int. Ed.*, 2025, **64**, e202415727.
13 X. Zhan, M. Li, S. Li, X. Pang, F. Mao, H. Wang, Z. Sun, X. Han, B. Jiang, Y. He, M. Li, Q. Zhang and L. Zhang, *Energy Storage Mater.*, 2023, **61**, 102875.
14 X. Li, J. Liang, X. Cao, S. Zhu, Y. Bai, J. Sun, H. Luo and J. Kong, *Rare Met.*, 2025, **44**, 2871–2899.
15 A. G. Nguyen and C. J. Park, *J. Membr. Sci.*, 2023, **675**, 121552.
16 L. Fan, S. Wei, S. Li, Q. Li and Y. Lu, *Adv. Energy Mater.*, 2018, **8**, 1702657.
17 W. Li, M. Li, S. Wang, P. H. Chien, J. Luo, J. Fu, X. Lin, G. King, R. Feng, J. Wang, J. Zhou, R. Li, J. Liu, Y. Mo, T. K. Sham and X. Sun, *Nat. Nanotechnol.*, 2025, **20**, 265–275.
18 R. Murugan, V. Thangadurai and W. Weppner, *Angew. Chem., Int. Ed.*, 2007, **46**, 7778–7781.
19 R. Dubey, J. Sastre, C. Cancellieri, F. Okur, A. Forster, L. Pompizii, A. Priebe, Y. E. Romanyuk, L. P. H. Jeurgens, M. V. Kovalenko and K. V. Kravchyk, *Adv. Energy Mater.*, 2021, **11**, 2102086.

20 Y. Chen, J. Qian, X. Hu, Y. Ma, Y. Li, T. Xue, T. Yu, L. Li, F. Wu and R. Chen, *Adv. Mater.*, 2023, **35**, 2212096.
21 J. Li, J. Chen, X. Xu, J. Sun, B. Huang and T. Zhao, *Energy Environ. Sci.*, 2024, **17**, 5521–5531.
22 J. Zhang, C. Wang, J. Fu, M. Ye, H. Zhai, J. Li, G. Tan, X. Tang and X. Sun, *Adv. Funct. Mater.*, 2024, **35**, 2416229.
23 D. Dai, P. Yan, X. Zhou, H. Li, Z. Zhang, L. Wang, M. Han, X. Lai, Y. Qiao, M. Jia, B. Li and D. Liu, *Green Carbon*, 2024, **2**, 310–315.
24 H. Li, Q. Lin, J. Wang, L. Hu, F. Chen, Z. Zhang and C. Ma, *Angew. Chem.*, 2024, **136**, e202407892.
25 M. S. Nafis, Z. Liang, S. Lee and C. Ban, *Nano Energy*, 2025, **133**, 110447.
26 L. Hu, Y. Ren, C. Wang, J. Li, Z. Wang, F. Sun, J. Ju, J. Ma, P. Han, S. Dong and G. Cui, *Adv. Mater.*, 2024, **36**, 2401909.
27 J. E. Trevey, J. Wang, C. M. DeLuca, K. K. Maute, M. L. Dunn, S. H. Lee and V. M. Bright, *Sens. Actuators, A*, 2011, **167**, 139–145.
28 B. Zhang, R. Tan, L. Yang, J. Zheng, K. Zhang, S. Mo, Z. Lin and F. Pan, *Energy Storage Mater.*, 2018, **10**, 139–159.
29 Z. Gao, H. Sun, L. Fu, F. Ye, Y. Zhang, W. Luo and Y. Huang, *Adv. Mater.*, 2018, **30**, 1705702.
30 Y. Huang, J. Zeng, S. Li, C. Dai, J. Liu, C. Liu and Y. He, *Adv. Energy Mater.*, 2023, **13**, 2203888.
31 G. Wang, H. Wu, M. Zheng, C. Zhao, J. Liang, L. Zhou, J. Yue, X. Zhu, Y. Xu, N. Zhang, T. Pang, J. Fu, W. Li, Y. Xia, W. Yin, X. Sun and X. Li, *Adv. Mater.*, 2024, **37**, 2410402.
32 W. Ji, D. Zheng, X. Zhang, T. Ding and D. Qu, *J. Mater. Chem. A*, 2021, **9**, 15012–15018.
33 X. Shi, Z. Jia, D. Wang, B. Jiang, Y. Liao, G. Zhang, Q. Wang, D. He and Y. Huang, *Adv. Mater.*, 2024, **36**, 2405097.
34 P. Zhai, N. Ahmad, S. Qu, L. Feng and W. Yang, *Adv. Funct. Mater.*, 2024, **34**, 2316561.
35 A. Du, H. Lu, S. Liu, S. Chen, Z. Chen, W. Li, J. Song, Q. Yang and C. Yang, *Adv. Energy Mater.*, 2024, **14**, 2400808.
36 S. Xu, K. Zhang, R. Xu, P. Tang, H. Cheng, Z. Sun and F. Li, *Energy Storage Mater.*, 2025, **74**, 103941.
37 H. An, M. Li, Q. Liu, Y. Song, J. Liu, Z. Yu, X. Liu, B. Deng and J. Wang, *Nat. Commun.*, 2024, **15**, 9150.
38 Y. Jiang, C. Xu, K. Xu, S. Li, J. Ni, Y. Wang, Y. Liu, J. Cai and C. Lai, *Chem. Eng. J.*, 2022, **442**, 136245.
39 Z. Jia, M. Jia, Q. Sun, N. Wang, Z. Bi and X. Guo, *Energy Storage Mater.*, 2024, **68**, 103325.
40 M. Lemaalem and P. Carbonniere, *Solid State Ionics*, 2023, **399**, 116304.
41 Q. Liu, G. Yang, X. Li, S. Zhang, R. Chen, X. Wang, Y. Gao, Z. Wang and L. Chen, *Energy Storage Mater.*, 2022, **51**, 443–452.
42 Y. Zhang, J. Li, M. Ge, Y. Huang and H. Xu, *Rare Met.*, 2024, **43**, 5625–5636.
43 X. Su, X. Xu, Z. Ji, J. Wu, F. Ma and L. Fan, *Electrochem. Energy Rev.*, 2024, **7**, 1–38.
44 J. Liu, Z. Wu, F. J. Stadler and Y. Huang, *Angew. Chem., Int. Ed.*, 2023, **62**, e202300243.
45 Y. Liu, X. An, K. Yang, J. Ma, J. Mi, D. Zhang, X. Cheng, Y. Li, Y. Ma, M. Liu, F. Kang and Y. He, *Energy Environ. Sci.*, 2024, **17**, 344–353.
46 S. Guo, Y. Su, K. Yan, C. Zhao, Y. Lu, H. Wang, J. Dong, N. Li, Y. Liu, Y. Guan, F. Wu and L. Chen, *Adv. Sci.*, 2024, **11**, 2404307.
47 X. Zhang, S. Cheng, C. Fu, G. Yin, L. Wang, Y. Wu and H. Huo, *Nano-Micro Lett.*, 2025, **17**, 2.
48 Z. Zhang, J. Guo, K. Cui, X. Zhang, Y. Yao, S. Wang and H. Wang, *Nano-Micro Lett.*, 2024, **16**, 181.
49 J. Hou, W. Sun, Q. Yuan, L. Ding, Y. Wan, Z. Xiao, T. Zhu, X. Lei, J. Lin, R. Cheacharoen, Y. Zhou, S. Wang, F. Manshaii, J. Xie, W. Li and J. Zhao, *Angew. Chem., Int. Ed.*, 2025, **64**, e202421427.
50 G. Polizos, M. Goswami, J. K. Keum, L. He, C. J. Jafta, J. Sharma, Y. Wang, L. T. Kearney, R. Tao and J. Li, *ACS Nano*, 2024, **18**, 2750–2762.
51 C. Liu, S. Wang, Z. Lu, J. Zhao, Y. Wu, C. Ren, R. Yang and C. Jin, *Nano Res.*, 2024, **18**, 94907087.
52 B. Luo, J. Wu, M. Zhang, Z. Zhang, X. Zhang, Z. Fang, Z. Xu and M. Wu, *Chem. Sci.*, 2023, **14**, 13067–13079.
53 W. Kong, Z. Jiang, Y. Liu, Q. Han, L. Ding, S. Wang and H. Wang, *Adv. Funct. Mater.*, 2023, **33**, 2306748.
54 R. Tong, Y. Huang, C. Feng, Y. Dong and C. Wang, *Adv. Funct. Mater.*, 2024, **34**, 2315777.
55 P. Zhao, Y. Wang, Q. Huang, Z. Jin and C. Li, *Angew. Chem., Int. Ed.*, 2025, **64**, e202416897.
56 K. Li, J. Huang, X. Qu, G. Fu, X. Chen, W. Shen and Y. Lin, *ACS Appl. Mater. Interfaces*, 2025, **17**, 3146–3162.
57 C. Shen, W. Feng, Y. Yu, H. Wang, Y. Cheng, C. Dong, J. Gu, A. Zheng, X. Liao, X. Xu and L. Mai, *Adv. Energy Mater.*, 2024, **14**, 2304511.
58 M. Cui, Y. Li, B. Jin, S. Sun and Q. Jiang, *Chem. Eng. J.*, 2024, **500**, 156748.
59 X. Wang, Z. Chen, X. Xue, J. Wang, Y. Wang, D. Bresser, X. Liu, M. Chen and S. Passerini, *Nano Energy*, 2025, **133**, 110439.
60 T. Wang, Z. Wang, H. Li, L. Cheng, Y. Wu, X. Liu, L. Meng, Y. Zhang and S. Jiang, *Carbon*, 2024, **230**, 119615.
61 Z. Wang, C. Zhao, N. Yao, Y. Lu, Z. Xue, X. Huang, P. Xu, W. Huang, Z. Wang, J. Huang and Q. Zhang, *Angew. Chem., Int. Ed.*, 2024, **64**, e202414524.
62 X. Zhang, S. Cheng, C. Fu, G. Yin, P. Zuo, L. Wang and H. Huo, *Adv. Energy Mater.*, 2024, **14**, 2401802.
63 D. Cao, X. Sun, Y. Li, A. Anderson, W. Lu and H. Zhu, *Adv. Mater.*, 2022, **34**, 2200401.
64 M. Li, S. Yang and B. Li, *Interdiscip. Mater.*, 2024, **3**, 805–834.
65 B. Chen, D. Xu, Z. Chang and A. Pan, *Adv. Sustainable Syst.*, 2024, **8**, 2400220.
66 D. L. Nelson, S. E. Sandoval, J. Pyo, D. Bistri, T. A. Thomas, K. A. Cavallaro, J. A. Lewis, A. S. Iyer, P. Shevchenko, C. V. Di Leo and M. T. McDowell, *ACS Energy Lett.*, 2024, **9**, 6085–6095.
67 F. Frie, H. Ditler, S. Klick, G. Stahl, C. Rahe, T. Ghaddar and D. U. Sauer, *ChemElectroChem*, 2024, **11**, e202400020.

68 S. Cangaz, F. Hippauf, F. S. Reuter, S. Doerfler, T. Abendroth, H. Althues and S. Kaskel, *Adv. Energy Mater.*, 2020, **10**, 2001320.
69 Y. Wang, T. Li, X. Yang, Q. Yin, S. Wang, H. Zhang and X. Li, *Adv. Energy Mater.*, 2023, **14**, 2303189.
70 X. Han, W. Zhou, M. Chen, J. Chen, G. Wang, B. Liu, L. Luo, S. Chen, Q. Zhang, S. Shi and C. Wong, *J. Energy Chem.*, 2022, **67**, 727–735.
71 L. Gu, J. Han, M. Chen, W. Zhou, X. Wang, M. Xu, H. Lin, H. Liu, H. Chen, J. Chen, Q. Zhang and X. Han, *Energy Storage Mater.*, 2022, **52**, 547–561.
72 L. Zhang, Y. Lin, X. Peng, M. Wu and T. Zhao, *ACS Appl. Mater. Interfaces*, 2022, **14**, 24798–24805.
73 W. Ping, C. Yang, Y. Bao, C. Wang, H. Xie, E. Hitz, J. Cheng, T. Li and L. Hu, *Energy Storage Mater.*, 2019, **21**, 246–252.
74 D. Cao, X. Sun, Y. Wang and H. Zhu, *Energy Storage Mater.*, 2022, **48**, 458–465.
75 D. Cao, T. Ji, A. Singh, S. Bak, Y. Du, X. Xiao, H. Xu, J. Zhu and H. Zhu, *Adv. Energy Mater.*, 2024, **13**, 2203969.
76 L. Hu, X. Yan, Z. Fu, J. Zhang, Y. Xia, W. Zhang, Y. Gan, X. He and H. Huang, *ACS Appl. Energy Mater.*, 2022, **5**, 14353–14360.
77 X. Xu, P. V. Evdokimov, V. S. Volkov, S. Xiong, X. Jiao, O. O. Kapitanova and Y. Liu, *Energy Storage Mater.*, 2023, **57**, 421–428.
78 J. Ma, S. Zhang, Y. Zheng, T. Huang, F. Sun, S. Dong and G. Cui, *Adv. Mater.*, 2023, **35**, 2301892.
79 Q. Liu, D. Zhou, D. Shanmukaraj, P. Li, F. Kang, B. Li, M. Armand and G. Wang, *ACS Energy Lett.*, 2020, **5**, 1456–1464.
80 S. Guo, T. Wu, Y. Sun, S. Zhang, B. Li, H. Zhang, M. Qi, X. Liu, A. Cao and L. Wan, *Adv. Funct. Mater.*, 2022, **32**, 2201498.
81 O. B. Chae and B. L. Lucht, *Adv. Energy Mater.*, 2023, **13**, 2203791.
82 Q. Liu and L. Wang, *Adv. Energy Mater.*, 2023, **13**, 2301742.
83 G. Lu, J. Nai, D. Luan, X. Tao and X. W. D. Lou, *Sci. Adv.*, 2023, **9**, 14.
84 Q. Xia, S. Yuan, Q. Zhang, C. Huang, J. Liu and H. Jin, *Adv. Sci.*, 2024, **11**, 2401453.
85 Z. Deng, S. Chen, K. Yang, Y. Song, S. Xue, X. Yao, L. Yang and F. Pan, *Adv. Mater.*, 2024, **36**, 2407923.
86 Y. Nomura and K. Yamamoto, *Adv. Energy Mater.*, 2023, **13**, 2203883.
87 W. Dachraoui, R. S. Kühnel, C. Battaglia and R. Erni, *Nano Energy*, 2024, **130**, 110086.
88 H. Liu, Y. Chen, P. H. Chien, G. Amouzandeh, D. Hou, E. Truong, I. P. Oyekunle, J. Bhagu, S. W. Holder, H. Xiong, P. L. Gor'kov, J. T. Rosenberg, S. C. Grant and Y. Hu, *Nat. Mater.*, 2025, **24**, 581–588.
89 M. Nagao, A. Hayashi, M. Tatsumisago, T. Kanetsuku, T. Tsudacd and S. Kuwabata, *Phys. Chem. Chem. Phys.*, 2013, **15**, 18600–18606.
90 P. Hartmann, T. Leichtweiss, M. R. Busche, M. Schneider, M. Reich, J. Sann, P. Adelhelm and J. Janek, *J. Phys. Chem. C*, 2013, **117**, 21064–21074.
91 R. Raj and J. Wolfenstine, *J. Power Sources*, 2017, **343**, 119–126.
92 W. Dachraoui, R. S. Kühnel, C. Battaglia and R. Erni, *Nano Energy*, 2024, **130**, 110086.
93 M. Nagao, A. Hayashi, M. Tatsumisago, T. Kanetsuku, T. Tsudacd and S. Kuwabata, *Phys. Chem. Chem. Phys.*, 2013, **15**, 18600–18606.
94 X. Gao, Z. Xing, M. Wang, C. Nie, Z. Shang, Z. Bai, S. Dou and N. Wang, *Energy Storage Mater.*, 2023, **60**, 102821.
95 Y. Liu, X. Xu, X. Jiao, O. O. Kapitanova, Z. Song and S. Xiong, *Adv. Mater.*, 2023, **35**, 2301152.
96 M. Jia, T. Wu, S. Zhang, S. Guo, Y. Fu and A. Cao, *Adv. Funct. Mater.*, 2024, **35**, 2415542.
97 G. Yang, X. Bai, Y. Zhang, Z. Guo, C. Zhao, L. Fan and N. Zhang, *Adv. Funct. Mater.*, 2023, **33**, 2211387.
98 L. Zhu, Y. Wang, Y. Wu, W. Feng, Z. Liu, W. Tang, X. Wang and Y. Xia, *Adv. Funct. Mater.*, 2022, **32**, 2201136.
99 K. Lee, E. Kazyak, M. J. Wang, N. P. Dasgupta and J. Sakamoto, *Joule*, 2022, **6**, 2547–2565.
100 D. Cao, T. Ji, A. Singh, S. Bak, Y. Du, X. Xiao, H. Xu, J. Zhu and H. Zhu, *Adv. Energy Mater.*, 2023, **13**, 2203969.
101 G. Yang, X. Bai, Y. Zhang, Z. Guo, C. Zhao, L. Fan and N. Zhang, *Adv. Funct. Mater.*, 2022, **33**, 2211387.
102 O. Sheng, H. Hu, T. Liu, Z. Ju, G. Lu, Y. Liu, J. Nai, Y. Wang, W. Zhang and X. Tao, *Adv. Funct. Mater.*, 2022, **32**, 2111026.
103 A. Banerjee, X. Wang, C. Fang, E. A. Wu and Y. S. Meng, *Chem. Rev.*, 2020, **120**, 6878–6933.
104 F. Sun, C. Wang, M. Osenberg, K. Dong, S. Zhang, C. Yang, Y. Wang, A. Hilger, J. Zhang, S. Dong, H. Markötter, I. Manke and G. Cui, *Adv. Energy Mater.*, 2022, **12**, 2103714.
105 H. Adenusi, G. A. Chass, S. Passerini, K. V. Tian and G. Chen, *Adv. Energy Mater.*, 2023, **13**, 2203307.
106 Y. Huang, B. Shao, Y. Wang and F. Han, *Energy Environ. Sci.*, 2023, **16**, 1569–1580.
107 K. Tao, W. He, A. Chen, Y. Han and J. Li, *Energy Storage Mater.*, 2025, **75**, 104034.
108 Z. Wan, X. Chen, Z. Zhou, X. Zhong, X. Luo and D. Xu, *J. Energy Chem.*, 2024, **88**, 28–38.
109 Y. He, C. Lu, S. Liu, W. Zheng and J. Luo, *Adv. Energy Mater.*, 2019, **9**, 1901810.
110 F. Sun, L. Duchêne, M. Osenberg, S. Risse, C. Yang, L. Chen, N. Chen, Y. Huang, A. Hilger, K. Dong, T. Arlt, C. Battaglia, A. Remhof, I. Manke and R. Chen, *Nano Energy*, 2021, **82**, 105762.
111 X. Wang, W. Hou, Y. Chen, Y. Yang, Y. Wang, Z. Guo, Z. Song and Y. Liu, *Adv. Energy Mater.*, 2024, **15**, 2402731.
112 Y. Mao, F. Mi, T. Wang and C. Sun, *Chem. Eng. J.*, 2024, **496**, 153823.
113 M. Sun, Z. Zeng, L. Peng, Z. Han, C. Yu, S. Cheng and J. Xie, *Mater. Today Energy*, 2021, **21**, 100785.
114 H. Gao, C. Lin, Y. Liu, J. Shi, B. Zhang, Z. Sun, Z. Li, Y. Wang, M. Yang and Y. Cheng, *Sci. Adv.*, 2025, **11**, eadt4666.
115 X. Xu, Q. Sun, Y. Li, F. Ji, J. Cheng, H. Zhang, Z. Zeng, Y. Rao, H. Liu, D. Li and L. Ci, *Small*, 2023, **19**, 2302934.
116 L. Zhang, Y. Lin, X. Peng, M. Wu and T. Zhao, *ACS Appl. Mater. Interfaces*, 2022, **14**, 24798–24805.

117 H. Huo, Y. Chen, N. Zhao, X. Lin, J. Luo, X. Yang, Y. Liu, X. Guo and X. Sun, *Nano Energy*, 2019, **61**, 119–125.
118 J. Wu, B. Pu, D. Wang, S. Shi, N. Zhao, X. Guo and X. Guo, *ACS Appl. Mater. Interfaces*, 2018, **11**, 898–905.
119 R. Xu, X. Zhang, X. Cheng, H. Peng, C. Zhao, C. Yan and J. Huang, *Adv. Funct. Mater.*, 2018, **28**, 1705838.
120 W. Yan, Z. Mu, Z. Wang, Y. Huang, D. Wu, P. Lu, J. Lu, J. Xu, Y. Wu, T. Ma, M. Yang, X. Zhu, Y. Xia, S. Shi, L. Chen, H. Li and F. Wu, *Nat. Energy*, 2023, **8**, 800–813.
121 C. Zheng, Y. Lu, Q. Chang, Z. Song, T. Xiu, J. Jin, M. E. Badding and Z. Wen, *Adv. Funct. Mater.*, 2023, **33**, 2302729.
122 W. Zhang, V. Koverga, S. Liu, J. Zhou, J. Wang, P. Bai, S. Tan, N. K. Dandu, Z. Wang, F. Chen, J. Xia, H. Wan, X. Zhang, H. Yang, B. L. Lucht, A. M. Li, X. Yang, E. Hu, S. R. Raghavan, A. T. Ngo and C. Wang, *Nat. Energy*, 2024, **9**, 386–400.
123 S. Xiong, Y. Liu, P. Jankowski, Q. Liu, F. Nitze, K. Xie, J. Song and A. Matic, *Adv. Funct. Mater.*, 2020, **30**, 2001444.
124 C. Sun, A. Lin, W. Li, J. Jin, Y. Sun, J. Yang and Z. Wen, *Adv. Energy Mater.*, 2020, **10**, 1902989.
125 Y. Ma, P. Qi, J. Ma, L. Wei, L. Zhao, J. Cheng, Y. Su, Y. Gu, Y. Lian, Y. Peng, Y. Shen, L. Chen, Z. Deng and Z. Liu, *Adv. Sci.*, 2021, **8**, 2100488.
126 B. Han, D. Feng, S. Li, Z. Zhang, Y. Zou, M. Gu, H. Meng, C. Wang, K. Xu, Y. Zhao, Ho. Zeng, C. Wang and Y. Deng, *Nano Lett.*, 2020, **20**, 4029–4037.
127 Z. Ju, C. Jin, H. Yuan, T. Yang, O. Sheng, T. Liu, Y. Liu, Y. Wang, F. Ma, W. Zhang, J. Nai and X. Tao, *Chem. Eng. J.*, 2021, **408**, 128016.
128 K. Lu, S. Gao, R. J. Dick, Z. Sattara and Y. Cheng, *J. Mater. Chem. A*, 2019, **7**, 6038–6044.
129 H. Liu, R. Tao, C. Guo, W. Zhang, X. Liu, P. Guo, T. Zhang and J. Liang, *Chem. Eng. J.*, 2022, **429**, 132239.
130 C. Wang, Y. Zhao, Q. Sun, X. Li, Y. Liu, J. Liang, X. Li, X. Lin, R. Li, K. R. Adair, L. Zhang, R. Yang, S. Lu and X. Sun, *Nano Energy*, 2018, **53**, 168–174.
131 H. J. Shin, J. T. Kim, D. Han, H. S. Kim, K. Y. Chung, J. Mun, J. Kim, K. W. Nam and H. G. Jung, *Adv. Energy Mater.*, 2024, **15**, 2403247.
132 Y. Yang, J. Wang, Z. Li, Z. Yang, B. Wang and H. Zhao, *ACS Nano*, 2024, **18**, 7666–7676.
133 F. Wu, Z. Wen, Z. Zhao, J. Bi, Y. Shang, Y. Liang, L. Li, N. Chen, Y. Li and R. Chen, *ACS Appl. Mater. Interfaces*, 2022, **14**, 38807–38814.
134 X. Zhuang, S. Zhang, Z. Cui, B. Xie, T. Gong, X. Zhang, J. Li, R. Wu, S. Wang, L. Qiao, T. Liu, S. Dong, G. Xu, L. Huang and G. Cui, *Angew. Chem., Int. Ed.*, 2023, **136**, e202315710.